Science and Technology of Advanced Materials

ISSN: 1468-6996 (Print) 1878-5514 (Online) Journal homepage: https://iom3.tandfonline.com/loi/tsta20

Solidification microstructures selection of Fe-Cr-Ni and Fe-Ni alloys

Takateru Umeda & Toshimitsu Okane

To cite this article: Takateru Umeda & Toshimitsu Okane (2001) Solidification microstructures selection of Fe-Cr-Ni and Fe-Ni alloys, Science and Technology of Advanced Materials, 2:1, 231-240, DOI: 10.1016/S1468-6996(01)00057-2

To link to this article: https://doi.org/10.1016/S1468-6996(01)00057-2

ELSEVIER

Science and Technology of Advanced Materials 2 (2001) 231–240

SCIENCE AND TECHNOLOGY OF ADVANCED MATERIALS

www.elsevier.com/locate/stam

Solidification microstructures selection of Fe–Cr–Ni and Fe–Ni alloys

Takateru Umeda*, Toshimitsu Okane

Department of Materials Science and Metallurgy, Graduate School of Engineering, The University of Tokyo, 7-3-1 Hongo Bunkyo-Ku, Tokyo 113-8656, Japan

Received 17 June 1999

Abstract

The transition of solidified phases in Fe–Cr–Ni and Fe–Ni alloys was investigated from low to high growth rate ranges using a Bridgman type furnace, laser resolidification and casting into a substrate from superheated or undercooled melt. The ferrite–austenite regular eutectic growth, which is difficult to find in typical production conditions of stainless steels, was confirmed under low growth rate conditions. The transition velocity between eutectic and ferrite cell growth had a good agreement predicted by the phase selection criterion. Which of either ferrite or austenite is easier to form in the high growth range was discussed from the point of nucleation and growth. Metastable austenite formation in stable primary ferrite composition was mainly a result of growth competition between ferrite and austenite. For a binary Fe–Ni system, a planar metastable austenite in the steady state, simultaneous growth such as eutectic and banded growth between ferrite and austenite in an initial transient region are confirmed. © 2001 Published by Elsevier Science Ltd.

Keywords: Fe–Cr–Ni alloy; Fe–Ni alloy; Phase selection; Metastable phase; Eutectic; Peritectic; Rapid solidification; Unidirectional solidification

1. Introduction

Stainless steels are still expanding in their uses for various applications to meet customers' demands. In a solidification processing expected to produce sound casts in a shape possibly close to that of the required products, their structure control is of great importance in accordance with the performances requested and reduction in production cost. To understand and control the solidification microstructures of stainless steels, two aspects are discussed: peritectic or eutectic transformation in low growth rate regimes; and metastable phase formation due to rapid solidification processing such as twin drum casting.

The phase diagram in the Fe–Cr–Ni ternary system is shown in Fig. 1(a). The monovariant line, which is the boundary between the ferrite and the austenite liquidus surfaces, shows the peritectic reaction near to the iron rich corner. However, for higher composition of chromium and nickel of over 15 mass% Cr and 10 mass% Ni, this monovariant line makes a eutectic trough. As shown in Fig. 1(b), which presents a transverse section of the phase diagram cut along the 70 mass% Fe constant line, the primary ferrite near to the eutectic monovariant line transforms to austenite, decreasing with temperature [1]. There are many reports about solidification microstructures formed in Fe–Cr–Ni stainless steels with the composition on both sides of the eutectic trough. The alloys on an austenite liquidus surface show the simple microstructures of austenite matrix grown as a primary phase and ferrite intermatrix, as expected from the solidification path. The ferrite primary solidification is more complicated, because the solid-state transformation occurs from ferrite to austenite with subsequent cooling after solidification shown in the phase diagram [2,3]. Ferrite–austenite eutectic is expected at the primary ferrite or primary austenite boundaries when the liquidus composition reaches the monovariant eutectic trough, according to the solidification path. However, there are few reports referring to this ferrite–austenite eutectic, especially in coupled growth. Therefore it is quite natural to ask why this eutectic has rarely been observed under normal solidification conditions. It is important to understand this eutectic reaction and to obtain its growth parameter, because of not only interest in the reaction itself, but also because of the distribution of austenite phase in the eutectic, which works as a starting point of the ferrite to austenite transformation in the normal solidification of primary ferrite composition. In the first of this report, the microstructure of unidirectionally solidified Fe–Cr–Ni alloys, of which the composition is located near to the eutectic trough, has been observed to confirm the ferrite–austenite coupled growth, and to investigate the conditions of this coupled growth.

In recent years large-scale rapid solidification processing of materials such as the strip casting of stainless steels has

* Corresponding author. Tel.: +81-3-5841-7158; fax: +81-3-5841-7177.
E-mail address: umeda@spl.mm.t.u-tokyo.ac.jp (T. Umeda).

1468-6996/01/$ - see front matter © 2001 Published by Elsevier Science Ltd.
PII: S1468-6996(01)00057-2

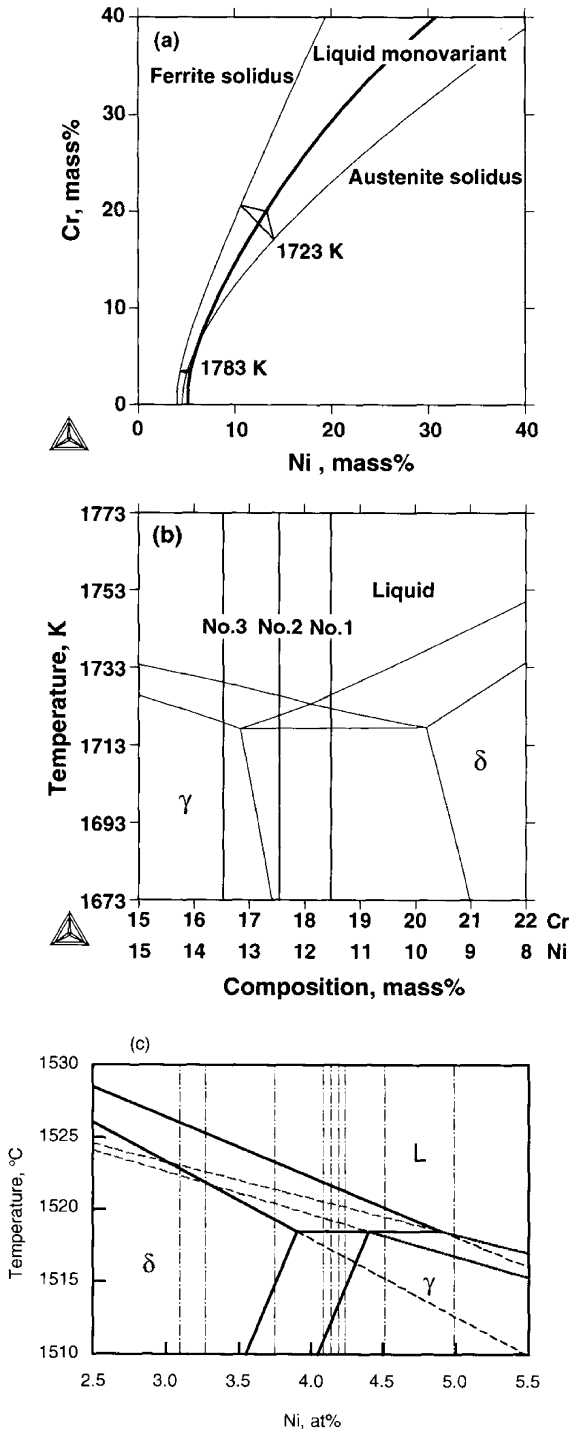

Fig. 1. Phase diagram in Fe–Cr–Ni system and composition of samples: (a) liquidus projection; (b) 70 mass% Fe transverse section and composition of typical samples used.

gained much interest [4]. Such processes lead to solidification velocities of up to several cm/s [5]. In such processes localization of diffusion and non-equilibrium phenomena and/or undercooling before solidification become important. Therefore a metastable phase may form instead of a stable phase. In 18–8 stainless steels under such rapid solidification conditions metastable austenite phase is easy to form [6]. A dendrite model including such growth conditions has been developed [7,8] and it has been shown to be of reasonable accuracy [9–11]. In this report the formation of metastable phases is discussed from the viewpoint of nucleation competition and growth competition between ferrite and austenite.

2. Primary phase estimation by the phase selection criterion

2.1. Interface response function of single phase

For analysis of the kinetically most stable phase/microstructure, the growth temperatures of all possible phases and growth morphologies must be known. These interface temperatures, which, for a given alloy, are a function of composition, growth velocity and temperature gradient, are called interface response functions. The relevant growth morphologies in the context of this discussion for single-phase directional solidification are plane front, cells and dendrites.

2.1.1. Single phase plane front growth

The growth temperature of a single-phase plane front assuming linear attachment kinetics and dilute solutions is given by [8,12,13]

$$T_p = T_m + C_l^* m_v - (R_g T_m/\Delta S_f)V/V_0, \quad (1)$$

where T_m is the melting temperature of the pure component, $C_l^* = C_0/k_v$ is the composition of the liquid at the interface, k_v is a velocity dependent distribution coefficient [14], m_v is the velocity-dependent liquidus slope defined by Boettinger and Coriell [12], R_g is the gas constant, ΔS_f is the molar entropy of fusion, and V_0 is the limit of crystallization, which has an upper bound equal to the velocity of sound. At steady state, T_p corresponds to the solidus temperature for the initial composition C_0. For more details of the calculations see Ref. [8].

The plane front temperature, T_p, is constant at low velocity: $T_p = T_s(\text{eq}) =$ solidus temperature. At high V, T_p first increases due to solute trapping, reaches a maximum close to T_0 of the alloy and then decreases because atom attachment kinetics become dominant (third term in the RHS of Eq. (1)). The maximum of T_p corresponds to the limit above which the plane front becomes unconditionally stable. Below this critical velocity, plane front growth is stable only when $V < V_c = GD/\Delta T_0$, the limit of constitutional undercooling. Between V_c and the absolute stability limit, $V_a = \Delta T_0(V)D/kG$, the plane front is morphologically unstable and it is replaced by a cellular/dendritic front. Between V_a and the maximum of the plane front temperature, banding occurs [15,16].

2.1.2. Dendritic/cellular growth

The growth temperature of dendrites can be written as [7,8]:

$$T_d = T_m - \Gamma K + C_l^* m_v - (R_g T_m/\Delta S_f)V/V_0, \quad (2)$$

Γ is the Gibbs–Thomson coefficient, K is the curvature of the dendrite tip, and C_l^* can be evaluated from the Ivantsov solution as $C_l^* = C_0/[1 - (1 - k_v)I(P_c)]$ [7]. Here P_c is the solutal Peclet number.

According to Burden and Hunt [17] the tip temperature for the low velocity regime where cells appear can be obtained from the following undercooling term:

$$\Delta T_c = GD/V. \quad (3)$$

It has been shown that this is a good approximation for cell growth undercooling [18,19]. The complete growth curve for directional cellular and dendritic growth can therefore be written as:

$$T_d = T_d^0 - \Delta T_c, \quad (4)$$

where T_d^0 is obtained from Eq. (2) with G equal to zero [7], the effect of the temperature gradient in the low velocity regime being introduced through ΔT_c.

For rates between V_c and V_a, the velocity range where the dendritic/cellular growth temperature is higher than that of the plane front, the growth temperature in the cellular regime first increases with V, then a transition to dendrites is observed which happens close to the maximum in T_d. In the dendritic regime solute rejection of the tips increases with V, leading to increased undercooling. At even higher V, a dendrite-to-cell transition is observed [18] and finally, at the limit of absolute stability, V_a, the cells disappear.

The alloys used in this report are essentially based on ternary Fe–Cr–Ni and more precise calculations were performed with the multi-component models [11,20,21].

2.2. Eutectic interface temperature calculation

The undercooling of ferrite–austenite eutectic coupled growth and microstructure spacing were calculated for a composition range near to the monovariant eutectic in the Fe–Cr–Ni ternary system. The interface temperature of the coupled growth, with a plane front interface, was calculated by subtracting this undercooling from the solidus temperature, i.e. the boundary between the monovariant liquid and related two-phase solids, corresponding to the initial composition.

2.3. Primary phase estimation by the phase selection criterion

A primary phase for the composition range on the 70 mass% Fe constant line in the Fe–Cr–Ni system was estimated. In this composition range, primary phase was expected among of ferrite, austenite, and coupled growth of these phases on monovariant eutectic as seen in the phase diagram. Primary phase was estimated by selecting the phase that has the highest interface temperature among the calculated interface response functions of all competitive phases. The data for calculation relating to the phase diagram were obtained using Thermo-Calc. Other properties for calculations are shown in Refs. [10,11].

2.4. Phase selection model

Eqs. (1) and (4) have to be solved numerically for all phases that compete in the process. For a given directional solidification condition, the kinetically most stable phase is then selected by the maximum growth temperature criterion. This approach leads to results for, for example, the three type of ferrite, austenite, and coupled growth of these phases in the Fe–Cr–Ni system.

3. Experimental procedure

Three types of solidification experiment were performed; unidirectional solidification of comparatively low growth rate using the Bridgman furnace; laser resolidification; and casting into a substrate from superheated or undercooled melt. Three compositions near to the eutectic trough for 70 mass% Fe of Fe–Cr–Ni alloys were prepared, as shown in Fig. 1(b) to investigate a unidirectional solidification structure map. The compositions used for other types of solidification experiment are very similar to those used for unidirectional solidification. Hypo-peritectic composition alloys of the binary Fe–Ni system are used to investigate formed phases, δ, γ, simultaneous and banded growth between δ and γ with planar morphology, considering the change from an initial transient to a stable state. The chemical compositions of Fe–Ni alloys are indicated as broken lines in the phase diagram, Fig. 1(c).

Unidirectional solidification was performed in an Ar atmosphere. The moving rate of the sample was changed from 1 to 500 μm/s and the temperature gradient at the solidification temperature range of the sample was 17 K/mm. The inner diameter of the alumina crucible is 6 and 8 mm for Fe–Cr–Ni and Fe–Ni alloys, respectively.

For a rapid solidification range, the following experiments were done: resolidification from a laser irradiated molten surface zone of steels; and an early stage of solidification cast into a substrate from undercooled or superheated melt. The capacity of the CO_2 laser machine was 3 kW. A single mode of irradiation was used with a power of 0.5, 1.0 and 1.5 kW and with a defocusing distance of 7.5–40 mm. The sample traveling speed was changed from 100 to 2000 mm/min.

An apparatus for melting by levitation or in a crucible and subsequent casting was set up. About 1 (3) g was levitation melted (in a silica tube), subsequently followed by cooling, generally: (i) to undercool from the liquidus temperature to some extent (hereafter called undercooled casting); (ii) in some cases to cast into a substrate before reaching the

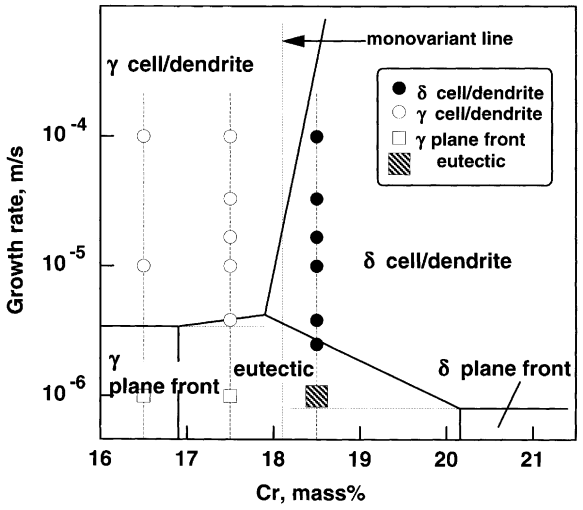

Fig. 2. Experimental results and estimated primary phase map by calculating the interface response function.

liquidus temperature (hereafter called superheated casting). A high response two-color eye thermometer and/or high-speed video camera monitored the undercooled melt. The undercooled melt before solidification or superheated melt was cast into a substrate in which the surface temperature of the steel through a hole (diameter 0.5 mm) was measured by a high response thermometer.

To detect the phases solidified, a standard metallographic technique was performed using 10 mass% sulfuric acid solution for electrolytic etching, and the solute distribution was measured by EPMA.

4. Experimental results

4.1. Unidirectional solidification microstructure in Bridgman furnace

Fig. 2 shows the solidification microstructure obtained under steady-state conditions. The indicated areas including solid line boundaries show solidification microstructures estimated by the phase selection criterion and interface response function calculation.

Solidification interface morphologies of a composition on the ferrite liquidus surfaces of sample No. 1 (Fe–18.5Cr–11.5Ni) are shown in Fig. 3. Fig. 3(a) shows an optical micrograph of a longitudinal section at a growth rate of 17 μm/s. At this growth rate, ferrite was solidified as primary phase with dendrite morphology. Austenite phase was occupied the space between ferrite dendrites. Ferrite transformed to austenite by solid state transformation with subsequent cooling, not by a peritectic reaction. Fig. 3(b) shows the microstructure of 2.5 μm/s, in which primary ferrite morphology changed to the cell structure as the growth rate became slower. Austenite appeared at the cell boundaries, and increased in volume fraction in the same

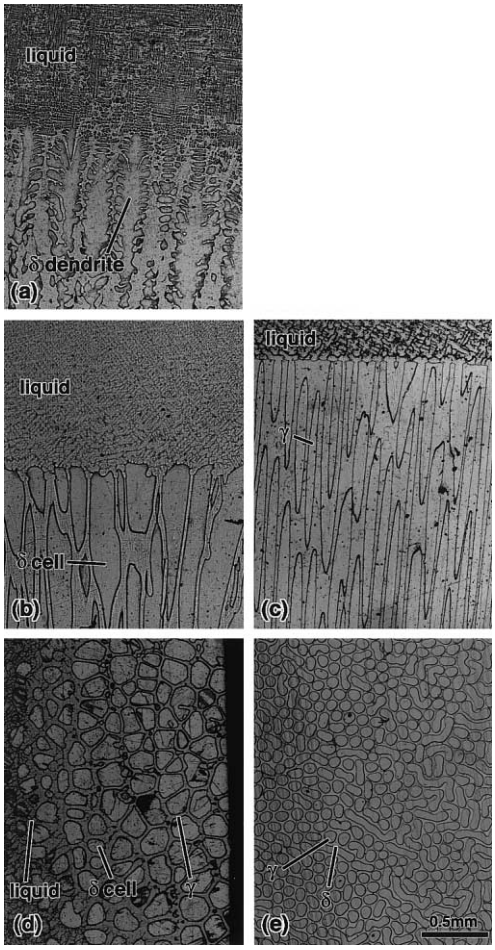

Fig. 3. Optical micrograph of unidirectional solidified Fe–18.5 mass% Cr–11.5 mass% Ni alloy. Growth rate: (a) 17 μm/s; (b)2.5 μm/s; (c) 1 μm/s; (d) 2.5 μm/s, transverse section of (b); (e) 1 μm/s; transverse section of (c).

way as for the case of higher growth rate. For lower growth rate, ferrite–austenite coupled growth at 1 μm/s was observed, as shown in Fig. 3(c).

It is clearer to see the difference between ferrite cell and coupled growth eutectic by observation of a transverse section cut near to the solidification macro solid/liquid interface. Fig. 3(d) is ferrite cell microstructure of 2.5 μm/s corresponding to Fig. 3(b). The solidification macro interface was convex along the temperature field of the apparatus. Thus in Fig. 3(d), the left side of this micrograph, the periphery of the transverse section of the rod sample, shows the microstructure quenched from liquid. The right side of this micrograph shows the perfectly solidified microstructure near to the center of the sample. Therefore, it is clear from this micrograph that ferrite was grown at first with cell structure, then austenite was grown at the cell boundary.

Fig. 3(e) shows the transverse section of 1 μm/s corresponding to Fig. 3(c), where ferrite and austenite phases both appear at the same time. It is noted that austenite takes a rod structure at this growth rate, as contrasted with the ferrite primary cell structure of 2.5 μm/s shown in Figs. 3(b) and (d).

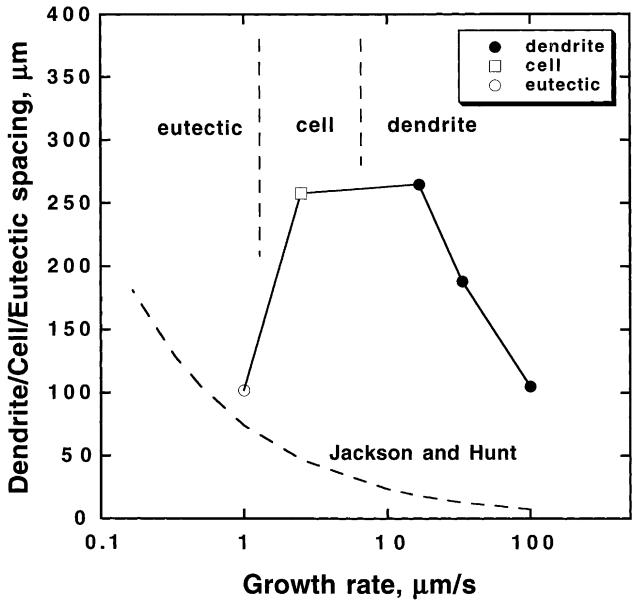

Fig. 4. Change of microstructure spacing with transition of phases and their morphologies in Fe–18.5 mass% Cr–11.5 mass% Ni alloy.

The solidification microstructure was changed with growth rates, e.g. ferrite dendrite, ferrite cell, rod eutectic structure, as mentioned before. Fig. 4 shows the spacing of these microstructures. The microstructure spacing became smaller with an increase of the growth rate in the ferrite dendrite solidification range. When the microstructure was changed from dendrite to cell, the spacing became a little smaller, as reported by Lu and Hunt [18]. For a lower growth rate range, when the microstructure was changed to eutectic structure, the eutectic spacing became smaller, about 1/3 as compared to cell spacing. The calculating eutectic spacing is also inserted in Fig. 4. The value of 100 μm of this rod structure had a good agreement with the value of 72 μm as calculated using the Jackson and Hunt theory [22].

The one reason among several why coupled growth in this system could only be observed under limited conditions, such as those in this report, and eutectic structures could not be observed at the inter-dendritic region, is assumed to be because of the large spacing of the eutectic. The eutectic rod spacing obtained, as large as 100 μm at a growth rate of 1 μm/s, is relatively large compared with the primary dendrite spacing of ferrite or austenite, and is a half to one-third of them, i.e. there is no space for the eutectic structure to form when the primary dendrite or cell has been grown, even though the conditions for eutectic growth are satisfied. The reason of this large eutectic spacing is related with the narrow eutectic composition range, as seen in the phase diagram. If the spacing of this monovariant eutectic could be estimated by the Jackson and Hunt method [22], which is, however, originally only applicable to binary eutectic, the large eutectic spacing in this system can be explained because this spacing is inversely proportional to the square root of the eutectic reaction isotherm.

4.2. Solidification microstructure in laser resolidification

Figs. 5(a)–(c) show the results of interface response function calculation for unidirectional solidification and laser resolidification. The transition velocity to appear as eutectic was estimated from Fig. 5(a), in which the transition between ferrite cellular growth and eutectic occurred, and this transition velocity had a good agreement with the experimental results as shown in Fig. 2. Contrarily, in the No. 2 sample shown in Fig. 5(b), the primary γ is stable. However, Although the eutectic was predicted, planar γ was formed, as shown in Fig. 2. This is probably due to a small temperature difference between γ and eutectic phases that results in difficulty of the δ nucleation necessary for the start of eutectic. At present, a nucleation event is difficult to predict.

Fig. 5(c) shows predicted interface temperatures of δ and γ, and compares them with experimental results for laser resolidification. The prediction was fairly good in this case, however, for some samples the predictions were not good. These discrepancies are not well understood at the present time and some reasons are considered such as improper estimation of growth rate, choice of physical properties according to changing of alloy composition and lack of data on calculating the phase diagram.

4.3. Casting into substrate from superheated and undercooled melts

Figs. 6(a) and (b) show micrographs of ingot surfaces obtained by casting from superheated and undercooled melts of Fe–18.5 mass% Cr–11.5 mass% Ni alloys, respectively. A superheat casting happens to form a metastable γ phase zone at the vicinity of the surface and transforms to a stable δ phase above this zone. This phenomenon was already reported by Mizukami et al. [6] in which undercooling over about 20°C at a surface forms a metastable γ, as shown in Fig. 7. Metastable γ formation, therefore, is a result of phase selection due to growth competition between δ and γ.

An undercooled casting produces a mixed structure of δ and γ which is observed at the surface zone and transforms to δ completely with decrease of growth rate (Fig. 6(b)). A substrate surface gives preferable sites to nucleate metastable γ because the undercooled melt of this composition prefers δ nucleation, shown in [23,24]. Therefore, mixed nucleation of δ and γ shows no nucleation competition between δ and γ.

Another aspect for phase selection between δ and γ of this composition must be considered, i.e. δ → γ transformation. If a tip temperature T^* is below $T_0(\delta/\gamma)$, which can easily happen because its line (surface) is located on a high enough temperature, already formed δ can transform to γ massively and rapidly. In this case visible γ is difficult to distinguish between γ transformed from original δ and originally nucleated and grown γ. Thus δ → γ transformation is

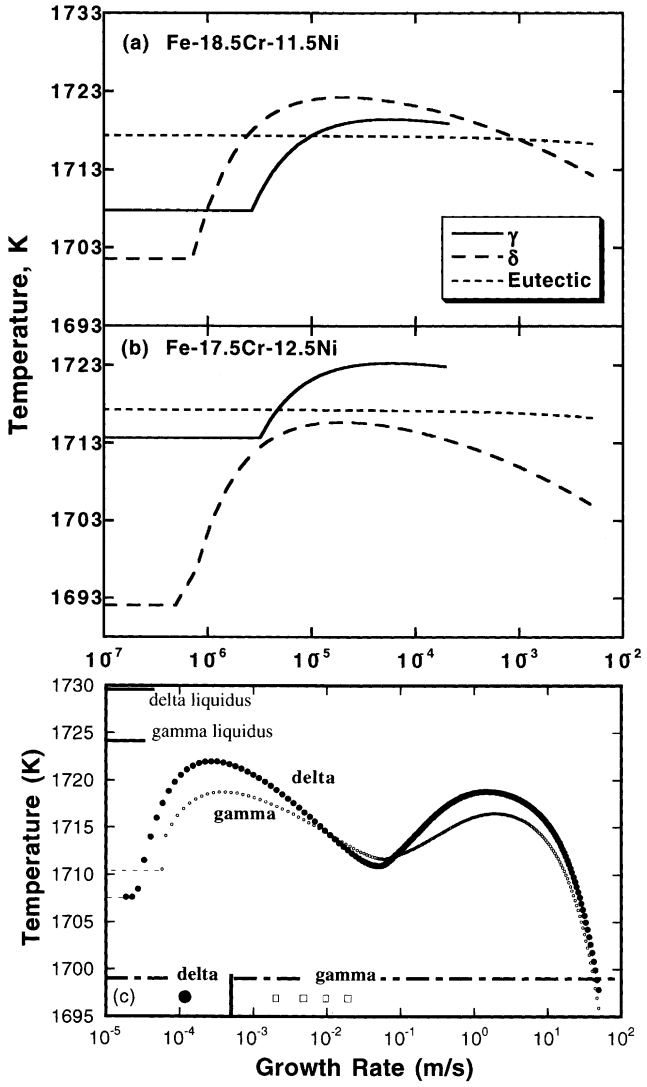

Fig. 5. Calculated interface response function: (a) low growth rate for unidirectional solidification in Fe–18.5 mass% Cr–11.5 mass% Ni alloy; (b) low growth rate for unidirectional solidification in Fe–17.6 mass% Cr–12.4 mass% Ni alloy; (c) laser resolidification in Fe–18.0 mass% Cr–10.9 mass% Ni alloy.

another possible candidate for the metastable γ formation mechanism along with growth competition.

4.4. Planar microstructures of hypo-peritectic Fe–Ni alloys; initial transient to steady state

Fig. 8 shows micrographs of 4.19 at% Ni alloy obtained by changing the quenching distance from an initial transient to a steady state under the growth rate of 1.5 μm/s. On this slow growth rate and high temperature gradient, a stable phase δ with a planar morphology crystallizes in the range of a shorter growth distance within an initial transient, shown in Figs. 8(a) and (b). Cellular γ is formed subsequently by the solid transformation in accordance with a temperature fall after δ planar solidification, and grows toward the δ/liquid interface. A longer growth distance from the beginning of solidification promotes a pile-up of solutes in front of a solid/liquid interface, which in turn results in decrease of the δ interface temperature and increase of the δ interface composition. As solidification progresses the γ tip temperature behind the δ/liquid interface increases owing to the change of the δ/liquid interface with a growth, indicated by the phase diagram and the

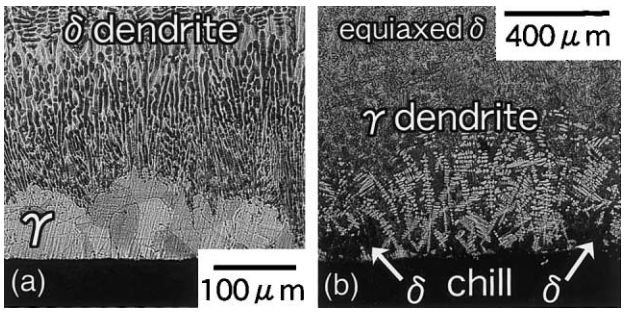

Fig. 6. Microstructures of casting into substrate from: (a) superheated melt; and (b) undercooled melt; of Fe–18.5 mass% Cr–11.5 mass% Ni alloy.

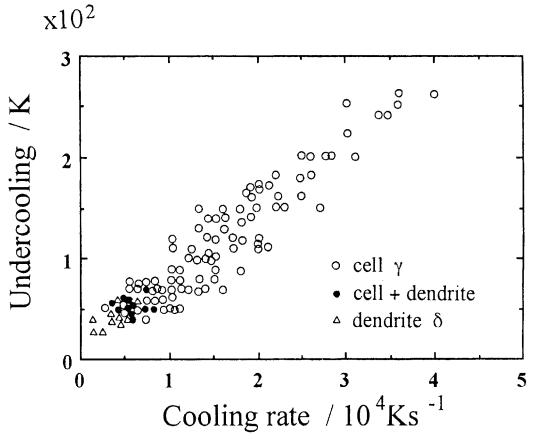

Fig. 7. Microstructure-phase selection map under the processing conditions of cooling rate vs. undercooling.

distance between fronts of δ and γ being closer. At a distance of 48 mm where a steady state attains, δ phase forms. Therefore at this hypo-peritectic composition a phase with higher interface temperature is selected, simply because a planar front temperature of the steady state is solidus and the solidus temperature of γ is higher than that of δ. Slower growth rates of 1.0 μm/s than that of Figs. 8 exhibits similar morphologies (Figs. 9(a) and (b)) but another type of morphology: simultaneous growth of δ and γ shown in Fig. 9(c). Fig. 10 shows a banded structure between δ and γ.

A change of interface morphologies with growth distance and growth rate is summarized in Fig. 11. The morphologies are still changing over a distance of $4D/kV$ estimated as an initial transient range, where D is the diffusion coefficient in the liquid, k is the equilibrium partition ratio and V is the growth rate. Simultaneous growth morphologies and banded structures are found just before steady growth starts.

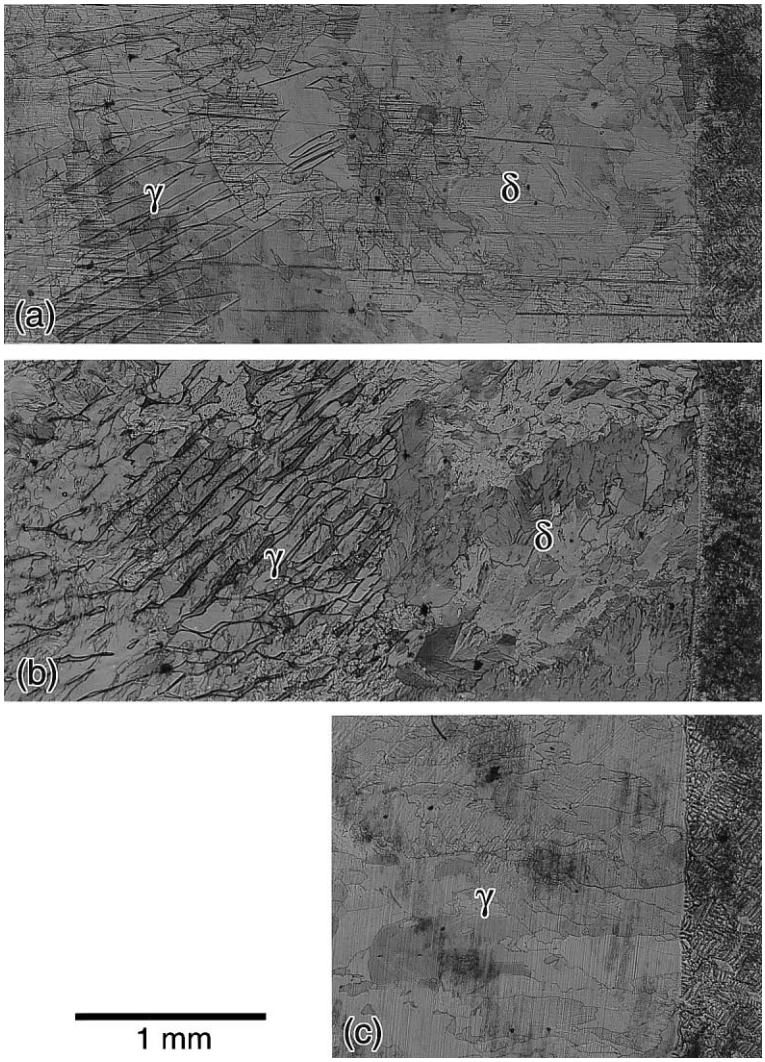

Fig. 8. Microstructures from an initial transient to a steady state of Fe–4.19 at% Ni alloys at a growth rate of 1.5 μm/s. Distance from the beginning of solidification; (a) 38 mm; (b) 44 mm; and (c) 48 mm, respectively.

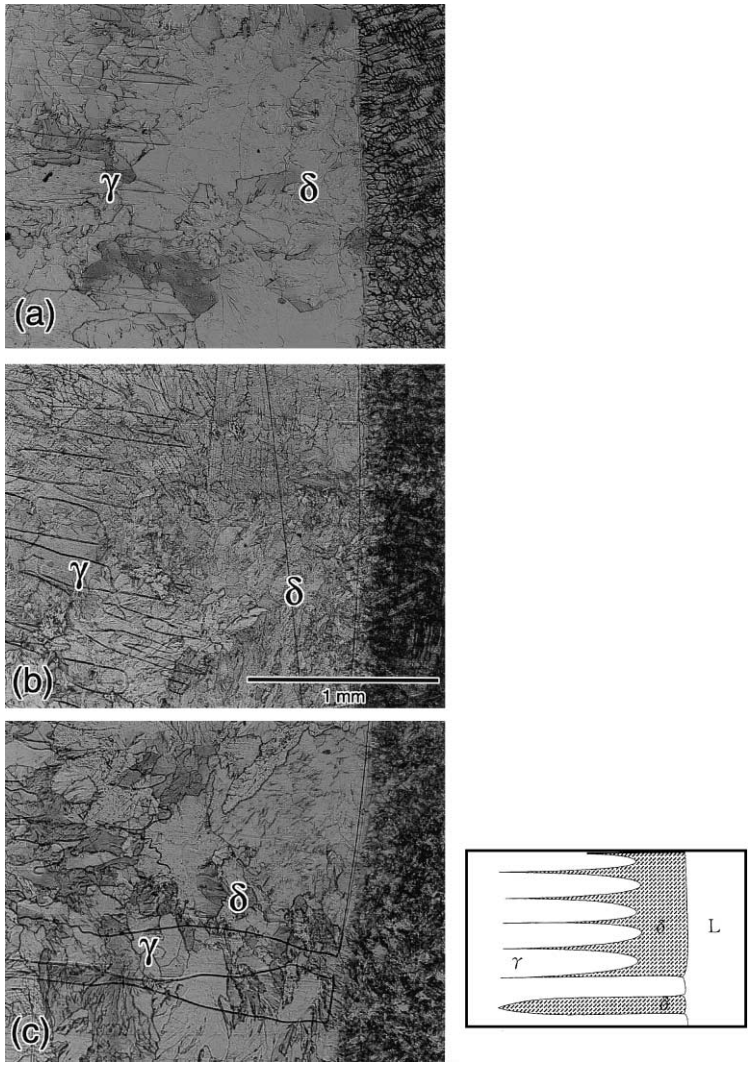

Fig. 9. Change of formed phases and its schematic illustration for Fe–4.19 at% Ni alloys at growth rate of 1.0 μm/s from the beginning of solidification (a) 42 mm; (b) 46 mm; and (c) 50 mm; respectively.

Nucleation of second phase on a planar primary phase is caused by two origins: (i) second phase nucleates on the primary phase at the solid/liquid interface; (ii) second phase starts to grow before nucleation when the tip of the transformed second phase catches up and is exposed on the solid/liquid interface as the initial transient advances.

A quantitative prediction as to which mechanism is dominant in terms of the nucleation of γ is made as follows. The Main assumptions are: (i) a nucleation temperature of γ on the δ/liquid interface, T_n, is given; (ii) the tip temperature of γ is determined by the supersaturation for the transformation from δ to γ, Ω.

T_n is evaluated as Eq. (5) from the reference of peritectic temperature, T_p:

$$T_n - T_p = \frac{m_\delta}{m_\delta - m_\gamma}\Delta T_{n\gamma}. \tag{5}$$

The tip temperature of γ, i.e. T_c, when the distance between a cellular tip γ and a planar δ/liquid interface is zero, is defined as Eq. (6) by using Ω:

$$T_c - T_p = \Omega\Delta C\left(\frac{1}{m_{s\delta}} - \frac{1}{m_{\delta+\gamma/\gamma}}\right)^{-1}. \tag{6}$$

The selection of the growth mode is assumed to be determined by the higher temperature of T_n or T_c. If $T_n > T_c$, γ does not catch up to the interface until the γ phase nucleates on the interface and starts to grow. This condition is expressed as Eq. (7):

$$\Omega > \left(\frac{1}{m_{s\delta}} - \frac{1}{m_{gd+\gamma/\gamma}}\right)\frac{m_\delta}{m_\delta - m_\gamma}\frac{\Delta T_{n\gamma}}{\Delta C}. \tag{7}$$

On the other hand, when $T_c > T_n$, the γ phase does not nucleate on the interface until the tip of γ phase transformed from δ phase catches up to the interface and the (γ phase

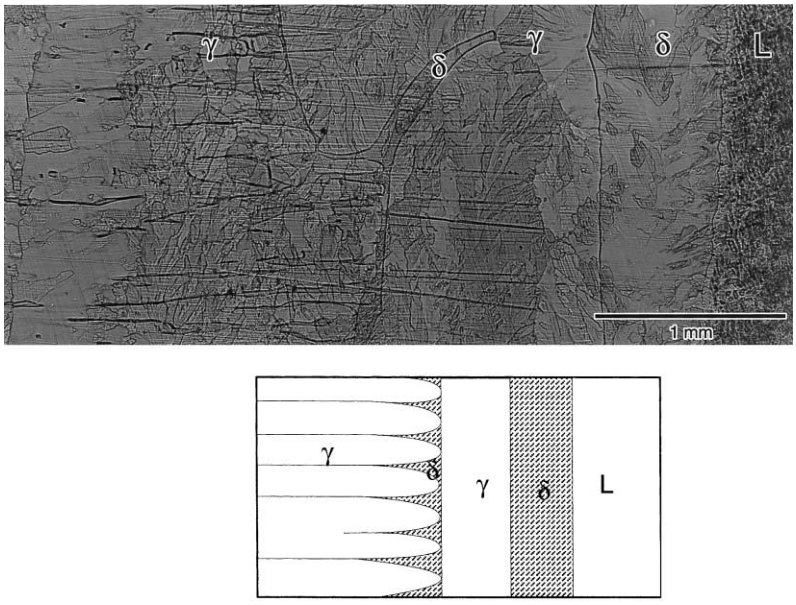

Fig. 10. Banded structure and its schematic illustration; Fe–4.24 at% Ni, growth rate of 1.7 μm/s, and a growth distance of 26 mm.

starts to grow. This condition is satisfied as Eq. (8):

$$\Omega < \left(\frac{1}{m_{s\delta}} - \frac{1}{m_{gd+\gamma/\gamma}}\right)\frac{m_\delta}{m_\delta - m_\gamma}\frac{\Delta T_{n\gamma}}{\Delta C}. \quad (8)$$

Parameters except supersaturation, Ω and undercooling for γ phase nucleation, $\Delta T_{n\gamma}$, are evaluated from the phase diagram. For eutectic of Fe–18.5Cr–11.5Ni (wt%) alloy, $\Omega = 0.025\Delta T_{n\gamma}$ is obtained, from which γ phase transformed from δ phase does not catch up to the interface unless the supersaturation for solid- transformation is very small. In fact Okane and Umeda [11] showed that eutectic does not begin to grow until γ nucleates on the δ/liquid interface. For the Fe–Ni system, on the other hand, $\Omega = 0.72\Delta T_{n\gamma}$ is obtained and Ω is evaluated to be 0.5 from the data of Vandyoussefi [25]. From this knowledge, unless undercooling for γ on the δ interface is comparatively smaller by 0.7 K, γ solidification does not occur to follow the (γ nucleation. When the undercooling necessary for γ on the δ interface is larger than 0.7 K, growing γ transformed from δ catches up with the δ/liquid interface at a later stage of initial transformation and γ starts to solidify. From observation of the simultaneous growth between δ and γ shown in Fig. 9, although in the peritectic system, and confirmation of the γ phase catch-up with the δ/liquid interface in Figs. 8 and 9, it can be concluded that simultaneous growth like that of lamella eutectic originates with the transformed cellular γ growth. At the same time, when γ nucleation occurs to small degree on the δ/liquid interface, a banded structure as shown in Fig. 10 may form.

5. Conclusions

To investigate the solidification microstructures selection of Fe–Cr–Ni and Fe–Ni alloys, three type of solidification experiment: low growth rate range using a Bridgman type furnace; high growth rate range obtained by laser resolidification; and casting into a substrate from superheated or undercooled melt; were performed.

1. Unidirectional solidification was performed to investigate the transition of the steady-state solidification microstructure of Fe–Cr–Ni alloys with growth rate. For the composition on the ferrite liquidus surface near to the monovariant eutectic line, ferrite–austenite eutectic is confirmed in the low growth rate range, and its transition velocity agreed well with that estimated by the phase selection criterion and calculation of interface

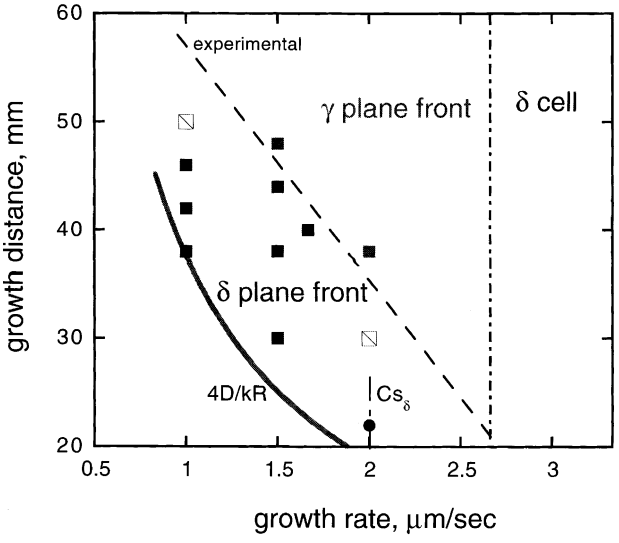

Fig. 11. Change of solidified phases and microstructures during an initial transient of Fe–4.19 at% Ni alloys.

response function. Eutectic follows nucleation of γ on the d/liquid interface.

2. Metastable austenite occurs by phase selection due to growth competition between austenite and ferrite. Critical undercooling or growth rate for transition from stable d to metastable g is well fitted with predictions.
3. Various kinds of microstructures of hypo-peritectic Fe–Ni alloys — planar/cellular/dendritic, peritectic/simultaneous (eutectic like), simultaneous/banded, stable/metastable — are formed according to the growth conditions. When nucleation events are specified, solidification-microstructures selection is quantitatively possible to predict from the standpoint of growth kinetics. Simultaneous growth is originated with γ catch-up with the δ/liquid interface and banded growth is caused by γ nucleation on the δ/liquid interface.

Acknowledgements

The authors would like to thank M. Hara, H. Kawabata and E. Takuma for their help to experiment and this work was partly supported by ISIJ Research Promotion Grant and the Kawasaki 21st Century Foundation.

References

[1] V. Raghavan, J. Phase Equilibria 15 (1994) 534.
[2] H.W. Kerr, Kurz, Int. Mater. Rev. 41 (1996) 129.
[3] J.A. Brooks, A.W. Thompson, Int. Mater. Rev. 36 (1991) 16.
[4] M. Cygler, M. Wolf, Iron Steelmaker 13 (1986) 27.
[5] H. Takeuchi, H. Nakashima, M. Yamada, S. Tanaka, Y. Yamakami, K. Yanagi, Steel Technol. Int. (1994) 181.
[6] H. Mizukami, T. Suzuki, T. Umeda, W. Kurz, Mater. Sci. Engng. A173 (1993) 361.
[7] W. Kurz, B. Giovanola, R. Trivedi, Acta Metall. 34 (1986) 823.
[8] R. Trivedi, W. Kurz, Int. Mater. Rev. 39 (1994) 49.
[9] Shu-Zu Lu, J.D. Hunt, P. Gilgien, W. Kurz, Acta Metall. Mater. 42 (1994) 1653.
[10] T. Umeda, T. Okane, W. Kurz, Acta Metall. Mater. 44 (1996) 4209.
[11] T. Okane, T. Umeda, ISIJ Int. 38 (1998) 454.
[12] W.J. Boettinger, S.R. Coriell, in: P.R. Sahm, H. Jones, C.M. Adams (Eds.), Science and Technology of the Undercooled Melt, NATO ASI Series E-No. 114, Martinus Nijhoff, Dordrecht, 1988, p. 81.
[13] M.J. Aziz, W.J. Boettinger, Acta Metall. Mater. 42 (1994) 527.
[14] M.J. Aziz, J. Appl. Phys. 53 (1982) 1158.
[15] M. Carrard, M. Gremaud, M. Zimmermann, W. Kurz, Acta Metall. Mater. 40 (1992) 983.
[16] W. Kurz, R. Trivedi, Metall. Trans. 27A (1996) 625.
[17] M.H. Burden, J.D. Hunt, J. Cryst. Growth 22 (1974) 109.
[18] Shu-Zu Lu, J.D. Hunt, J. Cryst. Growth 123 (1992) 17.
[19] W. Kurz, R.N. Grugel, Mater. Sci. Forum 77 (1991) 185.
[20] M. Bobadilla, J. Lacaze, G. Lesoult, J. Cryst. Growth 89 (1988) 531.
[21] M. Rappaz, S.A. David, J.M. Vitek, L.A. Boatner, Metall. Trans. 21A (1990) 1767.
[22] K.A. Jackson, J.D. Hunt, Trans. Met. Soc. AIME 236 (1966) 1129.
[23] T. Koseki, M.C. Flemings, Metall. Mater. Trans. A 26A (1995) 2991.
[24] T. Volkmann, W. Loser, D.M. Herlach, Metall. Mater. Trans. A 28A (1997) 461.
[25] M. Vandyoussefi, PhD thesis, EPFL, 1997.